

H.265/HEVC Video Steganalysis Based on CU-Block Structure Gradients and IPM Mapping

Xiang Zhang, Haiyang Xia, Ziwen He, Wenbin Huang, Fei Peng, Zhangjie Fu*

Abstract—Existing H.265/HEVC video steganalysis research mainly focuses on statistical feature modeling at the levels of motion vectors (MV), intra prediction modes (IPM), or transform coefficients. In contrast, studies targeting the coding-structure level—especially the analysis of block-level steganographic behaviors in Coding Units (CUs)—remain at an early stage. As a core component of H.265/HEVC coding decisions, the CU partition structure often exhibits steganographic perturbations in the form of structural changes and reorganization of prediction relationships, which are difficult to characterize effectively using traditional pixel-domain features or mode statistics. To address this issue, this paper, for the first time from the perspective of CU block-level steganalysis, proposes an H.265/HEVC video steganalysis method based on CU block-structure gradients and intra prediction mode mapping. The proposed method constructs a CU block-structure gradient map to explicitly describe changes in coding-unit partitioning, and combines it with a block-level mapping representation of IPM to jointly model the structural perturbations introduced by CU-level steganographic embedding. On this basis, we design a Transformer network, GradIPM-Former, tailored for CU-block steganalysis, thereby effectively enhancing the capability to perceive CU-level steganographic behaviors. Experimental results show that under different quantization parameters and resolution settings, the proposed method consistently achieves superior detection performance across multiple H.265/HEVC steganographic algorithms, validating the feasibility and effectiveness of conducting video steganalysis from the coding-structure perspective. This study provides a new CU block-level analysis paradigm for H.265/HEVC video steganalysis and has significant research value for covert communication security detection.

Index Terms—H.265/HEVC steganalysis, intra prediction modes, coding unit, Transformer.

I. INTRODUCTION

WITH the rapid development of multimedia technologies, massive amounts of information are transmitted over networks. Video steganography is a technique that enables covert transmission by hiding secret information in videos, and it is widely used in fields such as national defense and the military. However, the abuse of this technology can

This work was supported in part by the National Natural Science Foundation of China under Grant 62202234, 62372128, 62401270, 62502215, U22B2062, 62172232; China Postdoctoral Science Foundation under Grant 2023M741778; Natural Science Foundation of Guangdong Province under Grant 2023A1515011575; Nanjing Major Science and Technology Special Project under Grant 202405002. (Corresponding author: Zhangjie Fu)

Xiang Zhang, Haiyang Xia, Daoyong Fu, and Zhangjie Fu are with the Engineering Research Center of Digital Forensics, Ministry of Education, Nanjing University of Information Science and Technology, Nanjing, Jiangsu 210044, China (e-mail: zhangxiang@nuist.edu.cn; 202412490784@nuist.edu.cn; fudymo@hotmail.com; fzj@nuist.edu.cn).

Fan Wang is with the Faculty of Science and Technology, University of Macau, Macau, 999078, China (e-mail: wangfan@um.edu.mo).

Fei Peng is with the School of Artificial Intelligence, Guangzhou University, Guangzhou, Guangdong 510006, China (e-mail: eepengf@gmail.com).

pose serious threats to public security. Accordingly, video steganalysis has emerged, which can effectively detect whether videos transmitted through a channel contain secret information, thereby preventing the delivery of malicious hidden messages. In general, video steganalysis needs to be integrated with video coding technologies. As one of the most mainstream coding standards, High Efficiency Video Coding (H.265/HEVC) offers significant advantages over the previous H.264/AVC standard, including higher compression efficiency, support for higher resolutions, and better network adaptability [4]. Therefore, H.265/HEVC-based video steganalysis has become a major research focus. Existing H.265/HEVC-based video steganalysis methods can be categorized according to the type of carrier information being analyzed: inter-frame information-based steganalysis, transform-residual coefficient-based steganalysis, and intra prediction mode-based steganalysis [1].

Inter-frame information-based steganalysis mainly identifies stego videos by detecting abnormal distributions of inter-frame syntax elements. For example, Li et al. [2] proposed a video steganalysis algorithm based on the probability distribution of PU partition modes. This method constructs a steganalysis feature vector by counting the probabilities of different PU partition modes. Dai et al. [3] proposed a PU-mapping-based video steganalysis algorithm, which maps each frame into a PU partition-mode image and then builds a multi-scale residual network to adaptively extract cross-scale steganalysis features. This method achieves good detection performance. Liu et al. [4] proposed an H.265/HEVC steganalysis method that combines motion-vector (MV) neighborhoods and candidate lists. It computes the rate-distortion differences between eight neighboring MVs and two candidate MVs, constructing a 40-dimensional explicit feature set for stego video detection and achieving promising results. Wang et al. [5] proposed a content-aware video segmentation steganalysis method. To capture statistical changes caused by MV embedding, the authors introduced an MV-flow-based video segmentation mechanism. Steganalysis features are extracted separately from each subsequence to train sub-classifiers, thereby improving overall detection performance. This method can effectively exploit statistical abnormalities in temporal features such as motion vectors, and it achieves strong performance in detecting typical embedding patterns.

Transform-residual-coefficient-based steganalysis typically extracts features such as the statistical distribution of frequency-domain coefficients, energy concentration, and directional variations, and then uses these features to determine whether secret information has been embedded in the coefficients. For example, Wang et al. [6] proposed a steganalysis

algorithm based on DCT coefficients. By analyzing the impact of embedding perturbations on video correlations, the method constructs discriminative features that combine intra-frame residual histograms and inter-frame temporal feature maps, and further enhances detection performance using residual distortion. Zhang et al. [7] proposed a video steganalysis algorithm based on deblocking filtering, demonstrating that embedding secret information into transform-quantized coefficients affects the deblocking filtering process. Based on this observation, they extracted the modification magnitude and frequency of the luminance component and constructed a 768-dimensional steganalysis feature set, achieving good detection performance. However, because transform residuals are highly sensitive to coding parameters, content complexity, and compression ratio, coefficient-based statistical features tend to degrade under strong compression or complex scenes, making it difficult to capture steganographic traces caused by subtle structural perturbations. Zhang et al. [8] analyzed the distortion of transform-coefficient steganography and its impact on pixels, and proposed an HEVC transform-coefficient steganalysis method combined with a convolutional neural network. However, this method does not sufficiently consider the video prediction process, which makes the steganalysis less direct and leads to lower performance at low payloads. Dai et al. [9] proposed an H.265/HEVC transform-coefficient steganalysis method based on concentrated error and attention mechanisms. By analyzing the concentrated-error phenomenon introduced by distortion-compensation steganography, they constructed a prediction-error map to improve the signal-to-noise ratio, and designed a deep network that integrates channel and spatial attention as well as inter-frame self-attention, enabling effective detection of low-payload transform-coefficient steganography.

Intra prediction mode (IPM)-based methods typically detect stego videos by analyzing the differences in intra prediction modes before and after steganography. An IPM-calibration-based video steganalysis algorithm was proposed, which constructs IPM-shift probabilities and SATD-shift distance features to detect stego videos. This method demonstrates good detection performance under different quantization parameters and payloads. Liu et al. [10] proposed an end-to-end steganalysis model based on intra prediction modes and motion vectors, termed the Noise Residual Convolutional Neural Network. They found that modifications to syntax elements ultimately introduce subtle pixel perturbations in reconstructed frames. Therefore, by combining globally initialized high-pass convolution kernels, the PTLU activation function, and steganalysis residual blocks, they capture such steganographic disturbances and successfully improve detection performance. Shen et al. [11] proposed a steganalysis method based on intra prediction unit structures. By computing the differences in the number and proportion of prediction units before and after re-compression, they constructed a six-dimensional feature set to detect structural damage caused by steganography. Cao et al. [12] further pointed out that IPM modifications significantly compromise the rate-distortion optimality of the original partition structure. Based on this observation, they proposed an 11-dimensional feature set based on differences in depth matrices before and after encoding, which shows a

certain detection capability under low quantization parameters.

At present, steganalysis research targeting coding units (CUs) is still at an early stage. Within the HEVC coding framework, where optimal rate-distortion decisions are central, the partition structure of a Coding Unit (CU) directly determines the organization of Prediction Units (PUs) and Transform Units (TUs). Its spatial distribution and hierarchical relationships have a decisive impact on coding efficiency and reconstruction quality. When a steganographic algorithm introduces embedding constraints during coding, it often inevitably undermines the original optimality of CU partitioning, causing steganographic perturbations to manifest as changes in block structures, reorganization of hierarchical relationships, or structural discontinuities. Such structural-level anomalies are more stable, yet they are difficult to capture using traditional pixel-domain features or statistics of a single syntax element. A limited number of existing studies have attempted to analyze structural destruction from perspectives such as PUs or depth matrices, but they typically rely on low-dimensional handcrafted features, which are insufficient to fully represent the complex spatial patterns of CU structural changes and lack the capability to holistically model the relationships among different CUs. Therefore, how to systematically characterize CU block-level steganographic behaviors from the coding-structure perspective and build steganalysis models that are sensitive to structural perturbations while maintaining strong generalization ability remains an open problem requiring further investigation.

To address the above issues, this paper investigates CU block-level structural steganalysis. We observe that steganographic embedding based on Coding Units (CUs) inevitably affects the selection of intra prediction modes (IPMs). When the CU partition structure changes, the sizes of prediction units and their available neighboring contexts change accordingly, which in turn leads to a re-selection of the optimal intra prediction mode. This phenomenon is intuitively illustrated in Fig.1. Fig.1(a) and Fig.1(b) present the IPM co-occurrence matrix distributions of the cover video and the stego video, respectively. It can be observed that the IPM distribution in the stego video changes significantly compared with that of the cover video, especially near the diagonal, where the co-occurrence relationships exhibit local shifts and diffusion. This indicates that CU block-level steganography indeed alters the spatial distribution characteristics of IPMs, thereby introducing perceptible perturbations at the prediction-mode level.

However, further analysis reveals that although the IPM distributions differ visually, the changes mainly manifest as structural adjustments in local regions rather than significant shifts in a global statistical sense. In practical steganalysis, conventional IPM-based methods typically rely on co-occurrence statistics, distribution histograms, or low-order moments computed over an entire frame or across all PUs. Such statistical aggregation largely weakens—or even cancels out—the discriminative information carried by local structural variations, which limits the detection capability of methods that rely solely on IPM distributions in CU block-level steganography scenarios. This leads to our first motivation: although CU steganography alters IPMs, block-level or global

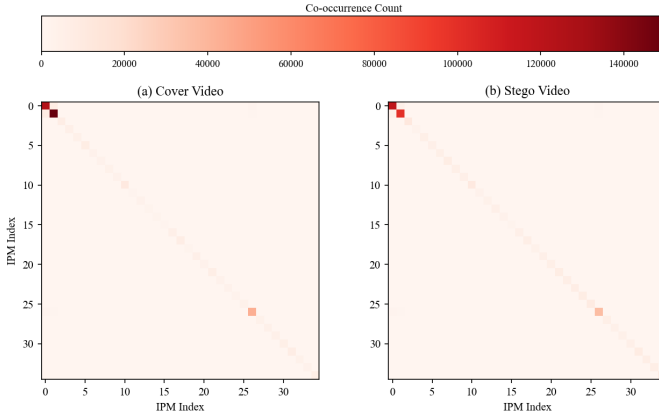


Fig. 1. Differences in IPM Co-occurrence Matrix Distributions Before and After CU Steganography

statistical features based only on IPMs are insufficient to stably capture such changes. Furthermore, we analyze deeper perturbations introduced by CU block-level steganography from the coding-structure perspective. We use the first frame from the “Aspen” sequence and construct the block-structure map and the block-structure gradient map (Dong et al. [17]) for both the cover and stego videos, as shown in Fig. 2 (left). We plot the cumulative distribution function (CDF) of the energy distribution based on the CU block-structure representation, and perform z-score normalization using the cover video as the reference. It can be seen that the overall CU-structure energy distributions of the stego and cover videos overlap closely, indicating that block-level mappings based solely on the number of CU structures or the proportions of hierarchical levels are also difficult to distinguish between cover and stego videos. In contrast, once gradient modeling is further applied to the CU block structure, the situation changes markedly. As shown in Fig. 2 (right), the stego video exhibits a much more pronounced overall shift in the structural-gradient distribution compared with the cover video. Structural gradients can directly characterize the intensity of CU block-boundary changes and are more sensitive to local structural discontinuities and changes in spatial organization.

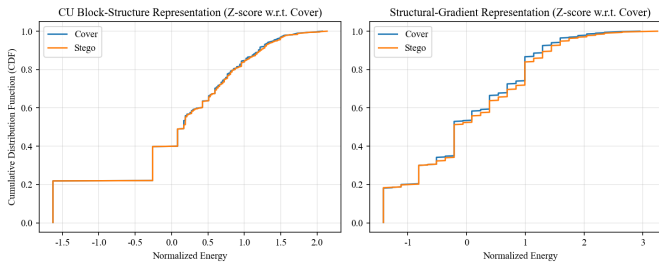


Fig. 2. Comparison of CDFs for Block-Structure Mapping and Block-Structure Gradient Mapping

Although CU block-level steganography remains stable in terms of global structural statistics, its interference with the rate-distortion optimal partitioning path introduces spatially consistent local structural perturbations, causing these anomalies to be effectively amplified in the structural-gradient do-

main. Therefore, our second motivation is that, compared with conventional block-structure mapping, CU structural-gradient mapping can capture the structural perturbations introduced by CU block-level steganography more sensitively, exhibiting stronger discriminative capability. Based on the above two observations, this paper takes a coding-structure perspective and jointly models CU block-structure gradients and IPM mapping features to achieve effective detection of CU-level steganographic behaviors.

Therefore, we propose an H.265/HEVC video steganalysis method based on CU block-structure gradients and intra prediction mode (IPM) mapping. Instead of focusing solely on value changes of a single syntax element, the proposed method explicitly models the coupling relationship between CU partition structures and prediction modes, and jointly characterizes the structural perturbations introduced by steganographic embedding. Specifically, we first construct a CU block-structure gradient map from coding information to capture the spatial partition boundaries and hierarchical changes of coding units. Meanwhile, we introduce a block-level mapping representation of IPM to reflect the distribution characteristics of prediction modes under CU-structure constraints. By aligning and fusing structural-gradient information with IPM-mapping information, the proposed method can more comprehensively describe the anomalous patterns introduced by CU-level steganographic embedding. Based on this, we design a Transformer network, GradIPMFormer, tailored for CU-block steganalysis. The network employs convolutional structures to extract local CU structural-change features, and further performs global modeling of long-range structural dependencies across CUs through sequence modeling and self-attention mechanisms, thereby enhancing the model’s ability to perceive complex structural perturbations. The main contributions of this paper are as follows:

- **A new perspective for H.265/HEVC video steganalysis targeting CU block-level steganographic behaviors is proposed.** Unlike existing steganalysis methods that mainly focus on statistical features of motion vectors, transform residual coefficients, or intra prediction modes, this work takes a coding-structure perspective and, for the first time, systematically investigates how CU block-level steganography affects coding decisions and the spatial organization of coding structures, providing a new research paradigm for HEVC video steganalysis.
- **A structural representation based on CU block-structure gradients were constructed.** It is used to characterize the structural perturbations introduced by steganographic embedding. We jointly model CU structural gradients and intra prediction mode (IPM) mapping to reveal the coupling relationship between them. Specifically, we further analyze how changes in CU partition structures affect the spatial distribution of IPMs, and construct an IPM mapping representation aligned with the CU structure. By jointly leveraging structural-gradient and IPM-mapping information, we can more comprehensively characterize the structural anomalies introduced by CU block-level steganographic embedding, thereby

compensating for the limitations of analyzing a single syntax element alone.

- **GradIPMFormer, tailored for CU-block steganalysis is proposed.** Given that CU structural changes exhibit long-range spatial dependencies and cross-block correlations, we design the GradIPMFormer architecture. The network combines convolutional feature extraction with self-attention modeling to globally capture structural relationships across CUs, thereby effectively enhancing the perception of complex CU-level steganographic behaviors.
- **Extensive experiments were conducted.** We conduct the effectiveness and robustness of the proposed method under diverse experimental settings. Experimental results across different quantization parameters, resolutions, network architectures, and multiple H.265/HEVC steganographic algorithms show that the proposed approach consistently achieves superior detection performance for CU block-level steganalysis, demonstrating the feasibility and effectiveness of conducting video steganalysis from the coding-structure perspective.

The remainder of this paper is organized as follows: Section II reviews preliminaries. Section III describes the proposed steganalysis model. Section IV discusses the experimental results and analysis. Finally, Section V is the conclusion.

II. PRELIMINARIES

A. Principles of Coding Unit (CU) Block Partitioning in H.265/HEVC

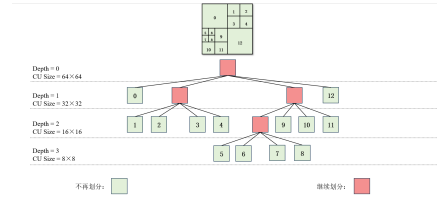


Fig. 3. CU Partition Structure in H.265/HEVC

In the H.265/HEVC coding standard, the Coding Unit (CU) is the basic building block of the intra-frame coding structure. Unlike the fixed macroblock structure in H.264/AVC, HEVC adopts an adaptive quadtree-based partitioning scheme to achieve finer rate-distortion optimization across different spatial regions. During encoding, each frame is first divided into multiple Coding Tree Units (CTUs), whose size is typically 64×64. For each CTU, the encoder recursively decides whether to further split it into smaller CUs, as shown in Fig. 3, and the partitioning process can be expressed as:

$$C = \left\{ CU_d^{(i)} \mid d = 0, 1, 2, 3 \right\} \quad (1)$$

where d denotes the depth level of the CU, and $CU_d^{(i)}$ represents the i -th CU at depth d . The CU partition decision is driven by the rate-distortion cost function (Rate-Distortion Cost), whose objective is to achieve an optimal trade-off

between distortion and bitrate. For any candidate CU partition scheme, its rate-distortion cost can be expressed as:

$$J = D + \lambda R \quad (2)$$

where D denotes the reconstruction distortion, R the number of bits required to encode the CU, and λ is the Lagrange multiplier related to the quantization parameter (QP). When the CU is further split, its total cost can be expressed as the sum of the costs of its sub-CUs, i.e.,

$$J_{\text{split}} = \sum_{k=1}^4 J_k \quad (3)$$

where J_k denotes the rate-distortion cost of the k -th sub-CU. The encoder compares J_{split} with the cost without splitting, J_{nosplit} , to determine whether to further split the current CU. Therefore, the CU partition structure essentially reflects the encoder's adaptive modeling of the spatial complexity of video content, and its spatial distribution exhibits prominent structural characteristics and hierarchical relationships.

B. Impact of CU Partition Changes on Intra Prediction Modes (IPM)

In the H.265/HEVC coding standard, intra prediction generates prediction samples for the current coding block by interpolation along specific directions. These predictions are obtained using reconstructed samples from the neighboring blocks above and to the left. The residual samples are then computed by subtracting the prediction samples from the original samples, thereby significantly reducing spatial redundancy. Compared with previous video coding technologies, H.265/HEVC greatly increases the number of intra prediction modes, providing a total of 35 modes. As shown in Fig. 4, these include planar prediction (mode 0), DC prediction (mode 1), and 33 directional prediction modes (modes 2–34). It should be noted that the selection of intra prediction modes

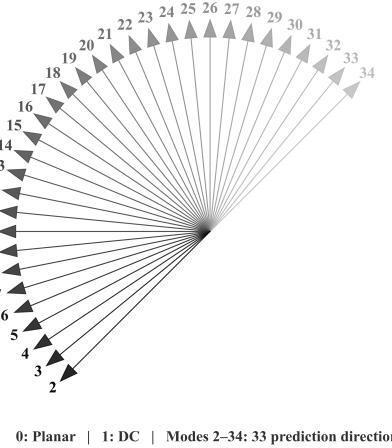


Fig. 4. Intra Prediction Modes in H.265/HEVC

strictly depends on the partition structure of the CU and its corresponding Prediction Units (PUs). For each leaf CU, the encoder needs to choose the optimal IPM from a set of

candidate prediction modes to minimize the rate–distortion cost. Let the candidate prediction mode set for a PU be:

$$\mathbf{M} = \{m_1, m_2, \dots, m_K\} \quad (4)$$

where K denotes the number of available IPM candidates. The finally selected prediction mode can be expressed as:

$$m^* = \arg \min_{m \in \mathbf{M}} (D(m) + \lambda R(m)) \quad (5)$$

where $D(m)$ and $R(m)$ denote the distortion and bitrate under prediction mode m , respectively. It should be noted that the optimality of the IPM is determined under the premise of a given CU partition structure. When the CU partition structure changes, the PU size, the available neighboring pixels, and the suitability of candidate prediction directions will all change accordingly, which may cause the originally optimal prediction mode to no longer satisfy the rate–distortion optimality condition.

Assume that under the cover (non-stego) condition, the partition structure of a CU is C_0 , and its corresponding optimal prediction mode is m_0 . When steganographic embedding introduces structural perturbations and the CU partition structure changes to C_1 , the corresponding optimal prediction mode becomes:

$$m_1 = \arg \min_{m \in \mathbf{M}} J(m \mid C_1) \quad (6)$$

It can be seen that even if the steganographic algorithm does not directly modify the IPM, its intervention in the CU partition structure may indirectly induce IPM reordering or shifts by altering the rate–distortion decision path. This phenomenon is intuitively illustrated in Fig. 1. (a) and Fig. 1.(b) present the IPM co-occurrence matrix distributions of the cover video and the stego video, respectively. It can be observed that the IPM distribution in the stego video changes noticeably compared with that of the cover video, especially near the diagonal, where the co-occurrence relationships exhibit local shifts and a diffusion trend. This indicates that CU block-level steganography indeed changes the spatial distribution characteristics of IPMs, thereby introducing perceptible perturbations at the prediction-mode level.

III. THE PROPOSED STEGANALYSIS MODEL

A. Overall Framework

The proposed H.265/HEVC video steganalysis method based on CU block-structure gradients and intra prediction mode mapping is illustrated in Fig. 5. From the coding-structure perspective, this framework targets the core objective of modeling structural perturbations caused by CU block-level steganographic behaviors, and consists of three main stages in sequence: coding information extraction, feature construction and joint modeling, and steganalysis classification.

B. CU Block-Structure Gradient Feature Construction and Alignment with Intra Prediction Mode Mapping Features

As discussed above, CU block-level steganographic embedding often introduces local anomalies at the coding-structure level by disrupting the original rate–distortion optimal partitioning path. To effectively model such structural perturbations, this paper starts from the CU partitioning results produced by the encoder to construct CU block-structure gradient features, and further performs pixel-level alignment with intra prediction mode (IPM) mapping to form a joint feature representation.

1) *CU Block-Structure Gradient Map Representation*: During H.265/HEVC encoding, each frame is partitioned into multiple Coding Units (CUs), and different CUs have different spatial sizes and hierarchical levels. Suppose the frame resolution is $H \times W$. For a pixel location (x, y) , let the size of the CU it belongs to be:

$$S(x, y) \in \{8, 16, 32, 64\} \quad (7)$$

Based on the CU partitioning results, we first construct a CU block-structure mapping map, as shown in Fig. 6, to represent the distribution of the coding structure at the pixel level:

$$C(x, y) = \log_2 \left(\frac{64}{S(x, y)} \right) \quad (8)$$

For an 8×8 CU that is further split into 4×4 PUs, it is represented as $C(x, y) = 4$.

However, as shown in Fig. 2, using only the CU-size mapping cannot explicitly characterize CU partition boundaries or their spatial discontinuities. To highlight regions of structural change, we further introduce CU block-structure gradient features to describe structural differences between the CUs to which neighboring pixels belong. For the CU structure map $C(x, y)$, the first-order discrete differences in the horizontal and vertical directions are defined as:

$$\Delta_x C(x, y) = \begin{cases} C(x, y) - C(x + 1, y), & x < W - 1, \\ 0, & x = W - 1, \end{cases} \quad (9)$$

$$\Delta_y C(x, y) = \begin{cases} C(x, y) - C(x, y + 1), & y < H - 1, \\ 0, & y = H - 1, \end{cases} \quad (10)$$

Based on this, we define the CU block-structure gradient magnitude using the L_1 -norm form as:

$$G(x, y) = \Delta_x C(x, y) + \Delta_y C(x, y) \quad (11)$$

This definition produces strong responses at CU partition boundaries while maintaining low values within CU interior regions, thereby effectively amplifying the structural discontinuities introduced by steganographic embedding. To eliminate the influence of numerical scale differences across different videos or frames, we apply max normalization to the structural-gradient features:

$$\hat{G}(x, y) = \frac{G(x, y)}{\max_{x, y} G(x, y) + \epsilon} \quad (12)$$

where ϵ is a small constant to avoid division by zero. The normalized structural-gradient feature $\hat{G}(x, y)$ facilitates subsequent network modeling.

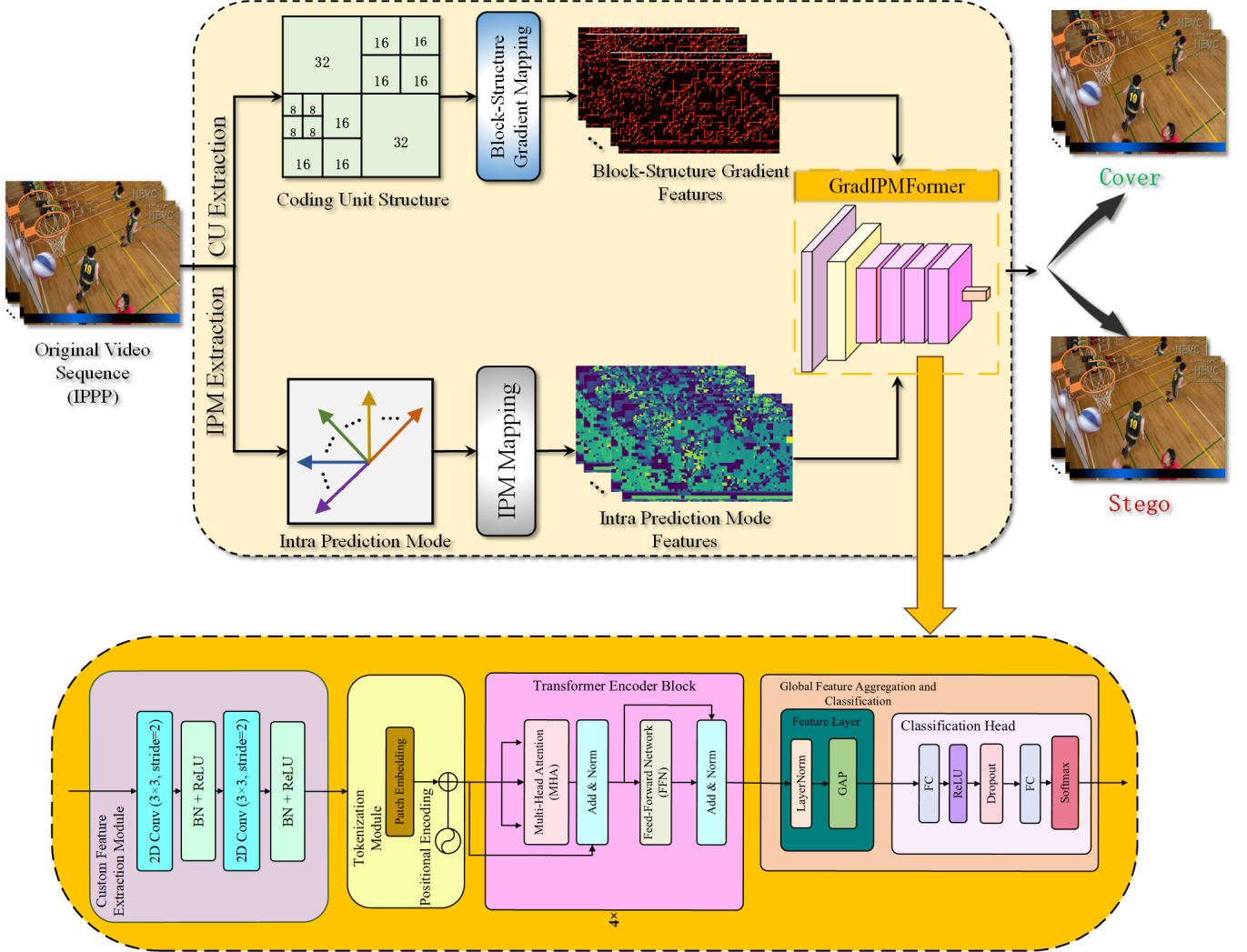
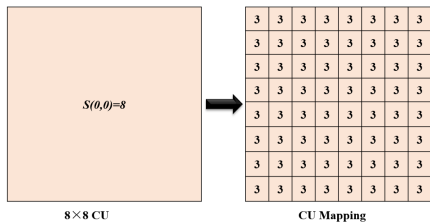


Fig. 5. The Proposed Steganalysis Framework

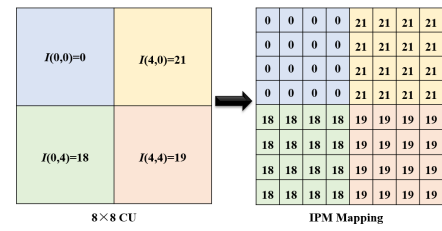
Fig. 6. Mapping of an 8×8 Coding Unit

2) Intra Prediction Mode (IPM) Mapping Construction:

In HEVC intra coding, each Prediction Unit (PU) corresponds to an intra prediction mode (IPM). Since IPM selection is directly constrained by the CU partition structure, its spatial distribution is highly correlated with the CU structure. To achieve spatial alignment with the CU structural gradients, we expand the original block-level IPM information into a pixel-level mapping representation. For a pixel location (x, y) , its IPM mapping is defined as:

$$I(x, y) = m_{CU(x, y)} \quad (13)$$

where $m_{CU(x, y)} \in 0, 1, \dots, 34$ denotes the intra prediction mode index of the CU to which the pixel belongs, as shown in Fig. 7. In our implementation, the IPM mapping map is stored

Fig. 7. Mapping of an 8×8 Coding Unit

as a 2D array and further normalized as:

$$\hat{I}(x, y) = \frac{I(x, y)}{34} \quad (14)$$

thereby constraining the IPM mapping values to the range $[0, 1]$. In addition, we also convert the IPM mapping into a

one-hot representation. For each pixel location (x, y) , its one-hot representation of the intra prediction mode is defined as:

$$\mathbf{e}_{I(x,y)} \in \mathbb{R}^{35} \quad (15)$$

where the $I(x, y)$ -th dimension of $\mathbf{e}_{I(x,y)}$ is set to 1 and all other dimensions are set to 0. This representation can, to some extent, avoid the implicit ordinal relationship among different IPM values.

3) *Pixed-Level Alignment and Fusion of CU Structural Gradients and IPM Mapping*: To jointly model CU block-structure perturbations and intra prediction mode variations, we adopt a pixel-level alignment strategy that establishes one-to-one correspondence between the structural-gradient features and the IPM-mapping features in the spatial domain, and fuses them along the channel dimension. Specifically, when using the one-hot representation, the joint feature tensor is defined as:

$$\mathbf{F}(x, y) = [\hat{G}(x, y), \mathbf{e}_{I(x,y)}] \in \mathbb{R}^{36} \quad (16)$$

Through the above procedure, we unify the CU structural-gradient features and IPM-mapping features into a multi-channel 2D feature map $\mathbf{F} \in \mathbb{R}^{36 \times H \times W}$, which serves as the input to the subsequent GradIPMFormer network.

C. Steganalysis Network: GradIPMFormer

To effectively model the complex perturbation patterns introduced by CU block-level steganographic behaviors at the spatial-structure level, we design a Transformer-based steganalysis network with joint inputs of structural gradients and intra prediction modes, termed GradIPMFormer. Structurally, the network consists of four components: a customized feature extraction module, a tokenization module, a Transformer encoder module, and a classification module. The overall framework is illustrated in Fig. 5.

1) *Customized Feature Extraction Module*: The input to GradIPMFormer is the joint feature tensor \mathbf{F} constructed in the previous section. Semantically, this input simultaneously contains CU structural-perturbation intensity information and prediction-mode distribution information, providing complementary structural cues for subsequent network modeling. Considering that CU structural perturbations exhibit strong locality in the spatial domain, GradIPMFormer first employs a lightweight 2D convolutional embedding module to perform local feature embedding on the input features. This module consists of two 3×3 convolutional layers, where the second layer performs downsampling with a stride of 2 to progressively reduce spatial resolution and enlarge the receptive field. For the input feature \mathbf{F} , the convolutional embedding process can be expressed as:

$$\mathbf{F}_1 = \sigma(\text{BN}(\text{Conv}_{3 \times 3}(\mathbf{F}))) \quad (17)$$

$$\mathbf{F}_2 = \sigma(\text{BN}(\text{Conv}_{3 \times 3}^{s=2}(\mathbf{F}_1))) \quad (18)$$

where $\text{Conv}_{3 \times 3}^{s=2}$ denotes a 2D convolution with stride 2, $\text{BN}(\cdot)$ denotes the batch normalization operation, and $\sigma(\cdot)$ is the ReLU activation function. Through this module, the network

can initially capture local perturbation patterns near CU structural boundaries, providing a foundation for subsequent patch-level modeling.

2) *Tokenization Module*: After obtaining the local feature map $\mathbf{F}_2 \in \mathbb{R}^{C' \times H' \times W'}$, GradIPMFormer further adopts a patch-embedding scheme to convert the 2D feature map into a sequential token representation. Specifically, a 2D convolution with stride equal to the patch size is used to perform non-overlapping patch embedding on the feature map:

$$\mathbf{Z} = \text{Conv}_{P \times P}^{s=P}(\mathbf{F}_2) \quad (19)$$

where P denotes the patch size. The resulting feature tensor \mathbf{Z} is reshaped into a token sequence as:

$$\mathbf{T} = [t_1, t_2, \dots, t_N], \quad t_i \in \mathbb{R}^D \quad (20)$$

where $N = \frac{H' \cdot W'}{P^2}$ is the number of tokens and D is the embedding dimension. To eliminate scale differences across channels, we apply Layer Normalization (LayerNorm) to each token:

$$\hat{t}_i = \text{LN}(t_i) \quad (21)$$

thereby obtaining a normalized token sequence:

$$\hat{\mathbf{T}} = [\hat{t}_1, \hat{t}_2, \dots, \hat{t}_N] \quad (22)$$

Since a Transformer lacks inherent awareness of spatial positional information, GradIPMFormer introduces learnable positional embeddings for each token to explicitly inject the spatial location of each patch in the original feature map. The positional embedding matrix is defined as:

$$\mathbf{P} \in \mathbb{R}^{N \times D} \quad (23)$$

The final input sequence fed into the Transformer encoder module is defined as:

$$\mathbf{T}_0 = \hat{\mathbf{T}} + \mathbf{P} \quad (24)$$

In this way, the model preserves the semantic consistency of tokens while gaining awareness of the spatial distribution of CU structural perturbations, providing a basis for the subsequent multi-head self-attention mechanism to model cross-CU structural correlations.

3) *Transformer Encoder Module*: GradIPMFormer employs a sequence modeling module composed of multiple stacked Transformer Encoder Blocks. Each Encoder Block consists of a Multi-Head Self-Attention (MHSA) module and a Feed-Forward Network (FFN), and uses residual connections and layer normalization to enhance training stability. For the l -th encoder block, the computation is:

$$\mathbf{T}'_l = \mathbf{T}_{l-1} + \text{MHSA}(\text{LN}(\mathbf{T}_{l-1})), \quad \mathbf{T}_l = \mathbf{T}'_l + \text{FFN}(\text{LN}(\mathbf{T}'_l)) \quad (25)$$

where the input token sequence to the l -th Transformer encoder block is $\mathbf{T}_l \in \mathbb{R}^{N \times D}$, N denotes the number of tokens,

and D denotes the feature dimension of each token. The multi-head self-attention mechanism is defined as:

$$\text{MHSA}(Q, K, V) = \text{Concat}(\text{head}_1, \dots, \text{head}_h) W^O \quad (26)$$

$$\text{head}_i = \text{Softmax}\left(\frac{QK^\top}{\sqrt{D}}\right) V \quad (27)$$

In the multi-head self-attention mechanism, the Query, Key, and Value matrices are first generated via linear projections:

$$Q = \mathbf{T}_{l-1} W^Q, \quad K = \mathbf{T}_{l-1} W^K, \quad V = \mathbf{T}_{l-1} W^V \quad (28)$$

where W^Q , W^K , and $W^V \in \mathbb{R}$ are learnable projection matrices. MHSA splits the feature dimension D into h attention heads, and the feature dimension of each head is:

$$d = \frac{D}{h} \quad (29)$$

The output of the i -th attention head, head_i , is computed by Eq. 27, where the scaling factor \sqrt{D} is used to alleviate numerical instability of dot-product attention in high-dimensional spaces. Finally, the outputs of all attention heads are concatenated and then linearly projected by $W^O \in \mathbb{R}^{D \times D}$ to obtain the MHSA output. Through MHSA, GradIPMFormer can explicitly model structural correlations among different CU regions and capture cross-CU collaborative perturbation patterns introduced by steganographic embedding.

4) *Global Feature Aggregation and Classification*: After Transformer encoding, global average pooling (GAP) is applied over all tokens:

$$\mathbf{f} = \frac{1}{N} \sum_{i=1}^N t_i^{(L)} \quad (30)$$

where L denotes the number of Transformer encoder layers, $t_i^{(L)}$ is the representation of the i -th token output by the L -th Transformer layer, and N is the total number of tokens. Through global average pooling (GAP), we aggregate the high-level structural representations of all tokens into a global feature vector \mathbf{f} , which is then fed into a multilayer perceptron (MLP) classifier to perform steganalysis classification:

$$\mathbf{y} = \text{Softmax}(W_2 \sigma(W_1 \mathbf{f})) \quad (31)$$

where W_1 and W_2 are the fully connected weight matrices in the MLP classifier, $\sigma(\cdot)$ denotes the ReLU non-linear activation function, and $\mathbf{y} \in \mathbb{R}^2$ represents the predicted probability distribution of the input video frame belonging to either the cover class or the stego class.

IV. EXPERIMENTAL RESULTS AND ANALYSIS

A. Experimental Setup

All experiments in this paper were conducted on a machine equipped with an NVIDIA GeForce RTX 4090 GPU, running at 3.1 GHz with 24 GB of memory. The proposed steganalysis algorithm was implemented in Python 3.11.

1) *Video Dataset*: The experiments use a video dataset constructed from 36 standard YUV video sequences, including 31 sequences with a resolution of 1920×1080 (1080P) and 5 sequences with a resolution of 832×480 (480P). The details of the dataset is shown in TABLE I. All the YUV sequences are obtained from the publicly available Xiph.org video test media (<https://media.xiph.org/>).

TABLE I
YUV TEST SEQUENCES

Index	Resolution	Sequence
1	832×480	BasketballDrill, BasketballDrillText, BQMall, PartyScene, RaceHorses, Aspen, BasketballDrive, BigBuckBunny, BlueSky, BQTerrace, Cactus, ControlledBurn, CrowdRun, Dinner, DucksTakeOff, ElephantsDream, Factory, InToTree, Kimono1, Life, OldTownCross, ParkJoy, ParkScene, PedestrianArea, RedKayak, Riverbed, RushFieldCuts, RushHour, SintelTrailer, SnowMnt, SpeedBag, Station2, Sunflower, TouchdownPass, Tractor, WestWindEasy
2	1920×1080	

For the 1080P videos, a total of 760 subsequences are generated, with each subsequence containing 60 frames. For the 480P videos, 47 subsequences are produced, each also consisting of 60 frames. In total, the dataset consists of 48,420 video frames. All YUV sequences follow the 4:2:0 format. To improve efficiency, all steganography algorithms in this study are implemented on the HM 16.15 platform. Therefore, the videos are encoded using HM 16.15 and subsequently decoded using HM 16.15. The GOP structure is configured as “IPPPPPPPPPPP” for 1080P videos and “IPPP” for 480P videos. It is worth noting that the “IPPP” configuration is adopted for the 480P videos because the number of available 480P source videos is significantly smaller than that of 1080P. A shorter GOP structure is needed to generate a relatively adequate number of samples.

2) *Steganography Methods*: To evaluate the detection performance of the proposed steganalysis algorithm, we employ four CU block-structure-based steganographic methods: Tew et al. [13] (denoted as Tar1), Dong et al. [14] (denoted as Tar2), Yang et al. [15] (denoted as Tar3), and Wang et al. [16] (denoted as Tar4).

3) *Setups for Performance Evaluation*: A total of five experimental setups are carefully designed to comprehensively evaluate the steganalytic performance, robustness, and cross-domain generalization of the proposed method.

Setup 1: Steganalysis under different QP settings. In this setting, we evaluate four representative H.265/HEVC steganographic algorithms under the same quantization configuration. Specifically, for each algorithm, video samples are encoded with QP values of 26, 32, and 38, and the embedding rate (payload) is set to 0.1 bpc (bits per cover), 0.3 bpc, and 0.5 bpc. We use two resolutions, 1080P and 480P, to comprehensively evaluate the proposed steganalysis detector under different spatial scales and compression strengths. For each steganographic algorithm, a separate steganalysis detector is trained and tested on its corresponding dataset.

Setup 2: Steganalysis comparisons. Since steganalysis research targeting coding unit (CU) block-structure steganography is still in its infancy, there are currently limited publicly available and reproducible baselines specifically designed for CU block-level steganographic behaviors. To ensure fairness and representativeness in the comparative experiments, we select three representative H.265/HEVC steganalysis methods as baselines, namely the methods of Cao et al. [12], Shen et al. [11], and Dai et al. [3]. These methods model abnormal variations of HEVC syntax elements from different perspectives, providing references for evaluating the advantages of our proposed method in terms of detection performance and robustness.

Setup 3: Comparison with different networks. To further verify the effectiveness and transferability of the proposed method across different detection architectures, we compare our approach with several representative networks, including NRNet [10], PUNet [3], ZhangNet [8], and CENet [9]. All competing methods are evaluated under the same data splits and evaluation protocols to ensure fairness and reproducibility. Specifically, under the configuration of Setting 1, we report the detection accuracy using the $QP = 32$ setting.

Setup 4: Robustness under mixed QP control and embedding conditions. This setting is designed to evaluate the robustness of our proposed method. We expect that the effectiveness of the steganalysis features used in our approach is less affected by the uniformity of the training data, which is beneficial when training data are limited. In this setting, the steganalyzer is built and tested using a mixture of video samples encoded with different rate-control modes and embedding strengths. All stego video samples are generated from Setting 1; specifically, we collect the 1080P and 480P stego video samples from Setting 1 separately and group them accordingly.

Setup 5: Generalization under the cover-source mismatch (CSM) setting. The CSM is considered one of the most critical factors hindering the practical deployment of steganalyzers. To simulate realistic detection scenarios, we train and test the steganalyzer using different video samples. Specifically, the training data consist of a mixture of 1080P video samples generated by Tar2 and Tar4 from Setting 1. The test data include 480P video samples generated by Tar1 and Tar3 obtained from Setting 3. Therefore, there are significant differences between the training and test sets in terms of embedding methods and resolution.

4) Training and Classification: For all setups (Setup 1–5), both cover and stego samples are randomly divided into training and testing sets at a ratio of 4:1. Meanwhile, a further 8:2 split is applied to the training set to form the training and validation subsets, which are used to monitor convergence and prevent overfitting. Training is conducted for 50 epochs using Adam optimizer (initial learning rate 1×10^{-4} , weight decay 1×10^{-4}). A ReduceLROnPlateau strategy is adopted to adjust the learning rate according to the validation loss. The loss function is the weighted cross-entropy, where class weights are dynamically computed based on the ratio of cover and stego samples to alleviate class imbalance. Automatic Mixed Precision (AMP) is employed to accelerate both forward and backward passes. The final performance is reported using the

model checkpoint that achieves the best validation accuracy and is evaluated on the independent testing set.

5) Performance Evaluation Index: The performance of the proposed steganalysis model is quantitatively assessed using standard evaluation metrics. In this study, classification accuracy is adopted as the primary metric to measure detection performance. The detection accuracy P_{ACC} is defined as:

$$P_{ACC} = \frac{TP + TN}{TP + TN + FP + FN} \quad (32)$$

where TP , TN , FP , and FN denote the numbers of true positives, true negatives, false positives, and false negatives, respectively.

B. Test Performances

1) Performance Evaluation of Steganalysis Under Different QP Settings: Table 2 reports the detection accuracy of the proposed method on four representative H.265/HEVC steganographic algorithms (Tar1–Tar4) under different quantization parameters (QPs) and payload settings. Experiments are conducted at two resolutions, 1080P and 480P, to evaluate steganalysis performance under different spatial scales and compression strengths. Overall, the detection accuracy shows a stable increasing trend as the payload grows. Under both resolutions and all QP configurations, increasing the payload from 0.1 to 0.5 leads to a significant improvement in detection performance for all steganographic algorithms, with accuracy reaching or even approaching 100% in some cases. This indicates that as embedding strength increases, the perturbations introduced by steganography to the coding structure and prediction decisions become more pronounced, and the proposed analysis method based on CU block-structure gradients and IPM mapping can effectively capture such structural anomalies. Further analysis of performance variations across different QP settings shows that detection performance is generally better at larger QP values (e.g., $QP = 38$) than in low-QP scenarios. Taking the 1080P resolution as an example, when QP increases from 26 to 38, the detection accuracy of Tar1–Tar4 under the same payload improves to varying degrees. This suggests that under strong compression, the encoder enforces stricter constraints on rate-distortion optimal structures, making steganographic embedding more likely to disrupt the optimality of the original CU partitioning and prediction modes, thereby introducing more salient abnormal patterns in both structural gradients and IPM distributions. In contrast, under low-QP conditions, the coding redundancy is higher, and steganographic perturbations are relatively more concealed at the structural level, which increases the detection difficulty accordingly.

In terms of resolution, the detection performance under the 1080P setting is overall higher than that under 480P. High-resolution videos contain more CU blocks and richer hierarchical structural information, allowing the perturbations introduced by steganographic embedding to CU partition structures and IPM distributions to be more fully manifested in the spatial domain. Although the detection accuracy slightly decreases at 480P, it remains at a high level in most configurations, indicating that the proposed method is robust to resolution

variations. From the perspective of different steganographic algorithms, Tar1 and Tar3 exhibit higher detectability in most experimental settings, whereas Tar4 yields relatively lower detection accuracy, especially under low-QP and low-payload conditions. This suggests that Tar4 performs embedding more cautiously with respect to perturbing the coding structure, making its steganographic traces more concealed. Nevertheless, even in this case, the proposed method can still achieve detection performance significantly better than random guessing under medium-to-high payloads and high-QP settings, validating the effectiveness of the joint modeling strategy based on CU block-structure gradients and IPM mapping in complex steganographic scenarios.

TABLE II
DETECTION PERFORMANCE($P_{ACC} \uparrow$) OF STEGANOGRAPHIC ALGORITHMS UNDER DIFFERENT QP AND PAYLOAD SETTINGS

Resolution	CQP	Steganography	Payload (bpc)		
			0.1	0.3	0.5
26	26	Tar1	89.67%	95.67%	100.00%
		Tar2	85.72%	90.66%	96.58%
		Tar3	88.82%	92.28%	99.80%
		Tar4	80.70%	86.32%	90.39%
1080P	32	Tar1	95.04%	99.61%	100.00%
		Tar2	92.22%	95.24%	97.11%
		Tar3	94.47%	96.05%	99.87%
		Tar4	86.46%	90.38%	95.11%
38	38	Tar1	97.37%	100.00%	100.00%
		Tar2	95.59%	97.63%	97.76%
		Tar3	96.34%	99.87%	99.65%
		Tar4	92.78%	95.30%	97.37%
26	26	Tar1	88.48%	93.43%	95.24%
		Tar2	82.62%	86.43%	89.71%
		Tar3	84.29%	86.19%	89.10%
		Tar4	76.67%	81.90%	85.76%
480P	32	Tar1	92.52%	95.38%	96.19%
		Tar2	85.38%	90.95%	93.05%
		Tar3	88.29%	90.48%	93.67%
		Tar4	83.81%	86.19%	90.71%
38	38	Tar1	95.92%	97.92%	100.00%
		Tar2	89.05%	93.67%	96.67%
		Tar3	90.67%	93.48%	96.48%
		Tar4	87.62%	90.71%	95.10%

Based on the above results, we can conclude that the proposed GradIPMFormer achieves stable and superior detection performance across different quantization parameters, resolutions, and multiple H.265/HEVC steganographic algorithms. The method can effectively leverage the joint perturbations introduced by steganographic embedding to coding-unit structures and prediction modes, providing a reliable solution for video steganalysis under complex coding conditions.

2) Comparison of Different Steganalysis Methods:

3) Comparison of Steganalysis Algorithms Across Four Different Networks:

4) Mixed QP control and embedding conditions Performance:

5) CSM Steganalysis Evaluation Performance:

C. Ablation Study

V. CONCLUSION

REFERENCES

- [1] S. Tan, F. Zheng, L. Liu, J. Han, and L. Shao, "Dense invariant feature-based support vector ranking for cross-camera person reidentification," *IEEE Transactions on Circuits and Systems for Video Technology*, vol. 28, no. 2, pp. 356–363, 2016.
- [2] Z. Li, L. Meng, S. Xu, Z. Li, Y. Shi, and Y. Liang, "A hevc video steganalysis algorithm based on pu partition modes," *Computers, Materials & Continua*, vol. 59, no. 2, 2019.
- [3] H. Dai, R. Wang, D. Xu, S. He, and L. Yang, "Hevc video steganalysis based on pu maps and multi-scale convolutional residual network," *IEEE Transactions on Circuits and Systems for Video Technology*, vol. 34, no. 4, pp. 2663–2676, 2023.
- [4] S. Liu, Y. Hu, B. Liu, and C.-T. Li, "An hevc steganalytic approach against motion vector modification using local optimality in candidate list," *Pattern Recognition Letters*, vol. 146, pp. 23–30, 2021.
- [5] P. Wang, Y. Cao, and X. Zhao, "Segmentation based video steganalysis to detect motion vector modification," *Security and Communication Networks*, vol. 2017, no. 1, p. 8051389, 2017.
- [6] P. Wang, Y. Cao, X. Zhao, and M. Zhu, "A steganalytic algorithm to detect dct-based data hiding methods for h. 264/avc videos," in *Proceedings of the 5th ACM Workshop on Information Hiding and Multimedia Security*, pp. 123–133, 2017.
- [7] H. Zhang, W. You, and X. Zhao, "A video steganalytic approach against quantized transform coefficient-based h. 264 steganography by exploiting in-loop deblocking filtering," *IEEE Access*, vol. 8, pp. 186862–186878, 2020.
- [8] Z. Zhang, H. Shi, X. Jiang, Z. Li, and J. Liu, "A cnn-based hevc video steganalysis against dct/dst-based steganography," in *International Conference on Digital Forensics and Cyber Crime*, pp. 265–276, Springer, 2021.
- [9] H. Dai, D. Xu, L. Yang, and R. Wang, "Hevc video steganalysis based on centralized error and attention mechanism," *IEEE Transactions on Multimedia*, 2025.
- [10] P. Liu and S. Li, "Steganalysis of intra prediction mode and motion vector-based steganography by noise residual convolutional neural network," *IOP Conference Series: Materials Science and Engineering*, vol. 719, no. 1, p. 012068, 2020.
- [11] Q. Sheng, R. Wang, M. Huang, Q. Li, and D. Xu, "A prediction mode steganalysis detection algorithm for hevc," *J Optoelectron-laser*, vol. 28, no. 4, pp. 433–440, 2017.
- [12] M. Cao, L. Tian, and C. Li, "A steganalytic approach to detect intra prediction mode modification using difference of partitioning structure for hevc," *IEEE Transactions on Consumer Electronics*, 2025.
- [13] Y. Tew and K. Wong, "Information hiding in hevc standard using adaptive coding block size decision," in *2014 IEEE international conference on image processing (ICIP)*, pp. 5502–5506, IEEE, 2014.
- [14] Y. Dong, X. Jiang, Z. Li, T. Sun, and P. He, "Adaptive hevc steganography based on steganographic compression efficiency degradation model," *IEEE Transactions on Dependable and Secure Computing*, vol. 20, no. 1, pp. 769–783, 2022.
- [15] L. Yang, D. Xu, J. Qian, and R. Wang, "Quad-tree structure-preserving adaptive steganography for hevc," *IEEE Transactions on Multimedia*, vol. 26, pp. 8625–8638, 2024.
- [16] S. Wang, D. Xu, and S. He, "Adaptive hevc video steganography based on pu partition modes," *Journal of Visual Communication and Image Representation*, vol. 101, p. 104176, 2024.